
**Undrained anisotropic monotonic behavior of sand from
in-situ tests**

Debasis Roy

Postal Address: Jacques Whitford and Associates
Ltd., Unit 1, 3771 North Fraser
Way, Burnaby, BC V5J 5G5, Canada.

E-mail: d_roy@look.ca

Telephone: 604 437 8141

FAX: 208 361 6451

Richard G. Campanella (Member)

University of British Columbia, Vancouver, BC.

Peter M. Byrne

University of British Columbia

John Hughes (Member)

Hughes In-Situ Engineering, Inc., Vancouver, BC.

ABSTRACT: A procedure for estimating undrained stress-strain behavior of sand from drained self-boring pressuremeter and seismic piezocone penetration tests is proposed in this paper. The procedure offers an inexpensive alternative to laboratory testing and avoids the uncertainty of the empirical methods based on index measurements such as the Standard Penetration Test (SPT) blow count and the tip resistance in a Piezocone Penetration Test (CPTU). To check its validity, the proposed procedure was used to infer the undrained triaxial stress-strain curves and the results were compared with laboratory triaxial tests on undisturbed samples. Undrained limit equilibrium stability of a dike was also assessed using the inferred stress-strain behavior to illustrate the usefulness of the procedure. The result of the stability analysis was found to be in qualitative agreement with the observed performance of the dike during a recent field experiment attempting to trigger static liquefaction.

INTRODUCTION

Since Arthur and Menezies (1972) and Oda (1972) demonstrated the significance of the influence of sample fabric on the mechanical response of sands, it became apparent that for a meaningful use of laboratory tests for prediction of field behavior it is necessary to test undisturbed samples. Due to the fact that extraction of undisturbed sand samples is usually very expensive, in-situ index measurements became popular tools for assessing undrained sand behavior. These methods use empirical correlations between an

index measurement, e.g., SPT $(N_1)_{60}$ or CPTU cone tip resistance (q_T), and the undrained strength, s_u . Figure 1 presents one such relationship between $(N_1)_{60}$ and s_u developed by Seed et al. (1988). The uncertainty in Seed's $(N_1)_{60}$ - s_u correlation is apparent from the wide spacing between the upper and lower bound curves. Attempts have been made to develop similar relationships using q_T (e.g., Figure 2) and the shear wave velocity, V_s (Fear and Robertson, 1994) instead of $(N_1)_{60}$. These relationships are not very precise either.

Although, not as common as an SPT or a CPTU, the Self-boring pressuremeter test (SBPMT) is in use since the 1970s. The advantages of the SBPMT are as follows:

- The measurements cover a wide range of deformation.
- The probe can be installed without causing appreciable disturbance in the soil surrounding the bore hole.
- The data can be analyzed from the principles of mechanics.

If a calibration procedure can be devised for a constitutive model using SBPMT data, the calibrated model may be useful in predicting the drained or undrained deformation behavior of sand. Such a method is expected to retain many of the advantages of the traditional approach based on laboratory tests on undisturbed samples without the cost implications of undisturbed sampling. This paper proposes such a calibration procedure for a stress-strain model based on SBPMT and CPTU measurements.

SELF-BORING PRESSUREMETER TESTING

In a self-boring pressuremeter test a cylindrical expandable probe (Figure 3) is installed in the ground by jetting, cutting or drilling. The installation procedure is optimized from a few initial trials to minimize the disturbance imparted on the soil around the probe. Once the probe is installed in the layer of interest, the expandable section (cavity) is inflated by pumping air or any other suitable fluid into the cavity at a regulated rate and tracking the cavity pressure and the corresponding deformation of the cavity wall. The deformation process can be analyzed from the principles of mechanics if the probe is long enough so that the deformed shape of the cavity is approximately cylindrical.

Figure 4 presents a plot between the cavity pressure and cavity strain from an SBPMT carried out at a site near San Francisco (Pass, 1994). Cavity strain, ϵ_0 , is defined as the ratio of the radial deformation of the cavity wall to the original cavity radius. The probe used was 83 mm in diameter, and 610 mm in length. The cavity deformation was monitored at three locations using three strain arms at each location. The location at the middle was at the central height of the cavity and the other two were 153 mm, or 1.83 times the probe diameter, above and below the central height. The cone tip resistance at an adjacent location (also shown on Figure 4) indicates that the probe was partly in loose soil ($q_T \approx 4$ MPa) and partly in a relatively dense stratum ($q_T \approx 8$ MPa) during the SBPMT. As a result, the top and the central strain arms measured a relatively softer response, while the lower

strain arm measurements were stiffer. Of interest is the fact that the influence of the stiffer layer around the bottom strain arm did not extend to the central height of the cavity. In other words, the zone of influence of soil stratification did not extend vertically beyond a distance of about 1.83 times the probe diameter from the interlayer boundary. It therefore appears that the central strain measurements may not be significantly affected by end fixity if the length of the expandable section exceeds 3.66 times its diameter. Examination of other SBPMTs in Pass' thesis leads to a similar inference. Cavity expansion data found elsewhere (e.g., Basudhar and Kumar, 1995; and Hughes et al., 1977) indicate that if the length to diameter ratio of the probe is 5 or more, the deformed cavity retains an approximately cylindrical shape near the central height for $\epsilon_0 \leq 0.1$. The probes used in this study had a length to diameter ratio of 5.6. Their deformation behavior were therefore approximated as a cylindrical process for cavity strains less than 0.1.

ANALYSIS OF CAVITY EXPANSION

The SBPMT data are usually back-analyzed to estimate soil parameters, e.g., the effective stress friction angle, ϕ' , the shear modulus, and the effective horizontal geostatic stress, σ_h' .

A simple approach of back analysis involves treating the parameters of interest (e.g., σ_h' and ϕ') as decoupled entities. Such methods sometimes (e.g., Hughes et al. 1977, and Yu, 1994) rely on analytically derived relationships between the slope of the

approximately linear section of the log-log plot between cavity pressure and ϵ_0 and the strength parameter of interest. Since the slope of the log-log plot is usually quite sensitive to installation related disturbance, the parameters back-figured from these methods are not always reliable (Bruzzi et al., 1992).

The other alternative is to treat the problem as an exercise of fitting a stress-strain model to SBPMT data for estimating a set of coupled soil properties. Such an approach – sometimes referred to as “curve fitting” – has been used by several investigators (e.g., Manassero, 1992; Fahey and Carter, 1994; da Cunha, 1994; Roy et al., 1996; Bahar et al., 1996). The same approach is used in this study as well. Experience at the University of British Columbia (UBC) with this approach indicates that the influence of installation related disturbance on derived strength parameters is minimized when measurements at cavity strain between 0.04 and 0.1 are relied upon (da Cunha, 1994).

The inverse problem in “curve-fitting” is usually under-determined. As a result, uniqueness of the solution is not guaranteed. The issue is qualitatively addressed here by using published correlations, supplementary soil test data and seismic CPTU measurements.

STRESS-STRAIN MODEL

An isotropic elastic double hardening plastic model is used in this research. A brief description of the model is as follows.

Elastic Behavior

The incremental stress-strain relationship for an isotropic elastic material is given by

$$d\varepsilon_{ij}^e = C_{ijkl}^e d\sigma_{kl}' \quad (1)$$

where ε_{ij}^e is the elastic strain, σ_{kl}' is the effective stress. The elastic compliance, C_{ijkl}^e , depends on the elastic tangent shear modulus, G_E , and the Poisson's Ratio, ν . The tangent shear modulus is assumed to depend on effective stress according to

$$G_E = K_{GE} P_A \left[\sigma_m / (P_A) \right]^{n_E} \quad (2)$$

where K_{GE} and n_E are model parameters, P_A is the atmospheric pressure and σ_m is the effective mean normal stress.

Modeling Plastic Behavior

For frictional materials in shear it can be shown from micromechanical principles that (Nakai and Matsuoka, 1983):

- yielding occurs when a change in stress results in an increase in the shear stress to effective normal stress ratio, η , on a special physical plane (called the Spatial Mobilized Plane or SMP) and
- η is a linear function of the ratio of the normal and shear components of the principal plastic strain increments on the SMP (called the strain increment ratio).

Constant- η surfaces, which assume an approximately conical shape with a non-circular cross section in the principal effective stress

space, thus represent the loading surfaces of this model (Figure 5). The component of principal plastic strain increments parallel to the SMP, γ_{SMP} , can be empirically related to η by

$$G_{PT} = n_A K_{SP} \left(\sigma_{SMP} / P_A \right)^{n_p} \left(1 - R_F \eta / \eta_F \right)^2 \quad (3)$$

and

$$\begin{aligned} n_A &= 1 - (m_A - 1) (2 \cos^2 \theta - 1) \text{ for } 90^\circ \leq \theta < 45^\circ \text{ and} \\ &= 1 \text{ for } \theta \geq 45^\circ, \end{aligned} \quad (4)$$

where G_{PT} is the tangential slope of the γ_{SMP} - η relationship, σ_{SMP} is the effective normal stress on the SMP, η_F is the ultimate (peak or failure) value of η , θ is the angle between the deposition direction and the unit normal to the SMP, and K_{SP} , R_F , n_p and m_A are model parameters. The linear relationship between the strain increment ratio and η and Eq. (3) represent the flow rule of this model. For the loading surface and the flow rule described above, an incremental stress-strain relationship of the following form can be derived (Roy, 1997)

$$d\varepsilon_{ij}^s = C_{ijkl}^s d\sigma_{kl}^s \quad (5)$$

where C_{ijkl}^s represents the shear compliance and is explicitly calculated from the knowledge of the following parameters:

- μ and $-\lambda$ denoting the intercept and the slope of the relationship between the strain increment ratio and η , respectively
- K_{SP} , R_F , n_p and m_A describing the γ_{SMP} - η relationship, and
- The value of η_F at $\sigma_m = P_A$ denoted by η_{F1} , and the change in the value of η_F for a ten-fold increase in σ_m denoted by $\Delta\eta$.

Isotropic Compression

To evaluate the plastic strain increment in isotropic compression, $d\varepsilon_{ij}^c$, an associated plasticity model proposed by Lade (1977) is used. The loading surfaces of this formulation are essentially a family of spheres in the effective principal stress space given by $f_c = \sigma_{ij}' \sigma_{ij}'$ (Figure 5). From the following empirical relationship between the plastic work in isotropic compression, W_c , and f_c

$$W_c = C P_A \left(f_c / P_A^2 \right)^p \quad (6)$$

it can be shown that the plastic strain increment for isotropic compression, $d\varepsilon_{ij}^c$, is given by

$$d\varepsilon_{ij}^c = \frac{C p}{2 f_c P_A} \left(\frac{f_c}{P_A^2} \right)^{p-1} \frac{\partial f_c}{\partial \sigma_{ij}'} \frac{\partial f_c}{\partial \sigma_{kl}'} d\sigma_{kl}' \quad (7)$$

Strain increments from Eqs. (1), (5), and (7) are added together to calculate the total strain increment.

APPROXIMATE MODEL CALIBRATION

The parameter K_{GE} depends mainly on the relative density, D_R , and can be determined from the from downhole seismic measurements for a given effective geostatic stress. For ordinary mineral sands with grains that cannot be crushed easily $n_E \approx 0.5$ and research of Tatsuoka and Kohata (1995), Lade and Nelson (1987) and Hardin (1978) suggest $\nu \approx 0.2$ is appropriate for sands. Typical values of K_{GE} and n_E of a few soil types have been summarized in Table 1.

Two triaxial compression, one triaxial extension, and two isotropic compression tests on undisturbed samples are ideally needed for evaluating the plastic parameters. Such an elaborate testing program is seldom feasible. An approximate method is therefore developed as described below.

Among the ten plastic parameters, K_{SP} , η_{F1} and μ have the most significant influence on model response in cylindrical cavity expansion as well as on the deformation behavior of a single triaxial or plane-strain element in compression or in extension. Figure 6 illustrates the influence of these parameters on cylindrical cavity expansion. Reasonably precise estimates of these parameters are therefore needed for satisfactory performance of the calibration method. Parameter K_{SP} is derived from back-analysis of SBPMT. For other parameters we proceed as follows in the absence of more precise material specific information.

Since η relates to the effective stress friction angle in triaxial compression, ϕ'_{TXC} , by

$$\eta = 2\sqrt{2} \tan \phi'_{TXC} / 3 \quad (8)$$

and ϕ'_{TXC} is mainly affected by the relative density, estimates of η_{F1} and $\Delta\eta$ follows from the knowledge of D_R . The ϕ'_{TXC} - D_R correlation developed by Bolton (1986) is utilized in this study. The relative density is inferred from the cone tip resistance following Robertson and Campanella (1986). The effect of fabric on ϕ'_{TXC} is less than $\pm 2.5\%$ (Tatsuoka et al., 1986). Therefore, the uncertainty due to the use of Bolton's relationship is expected to be minor. To allow for the influence of impeded drainage on

Roy et al.

boundary energy, the following empirical relationship is used (Roy, 1997)

$$\left(\tan\phi'_{\text{TXC}} - \tan\phi_{\text{cv}}\right)_{\text{Undrained}} = 0.46 \left(\tan\phi'_{\text{TXC}} - \tan\phi_{\text{cv}}\right)_{\text{Drained}} \quad (9)$$

where ϕ_{cv} is the constant volume effective stress friction angle.

Parameters λ and μ are not affected by sampling disturbance, stress level or stress path. Ideally therefore λ and μ should be evaluated from a suitable laboratory test, e.g., triaxial compression, using reconstituted specimen. In the absence of such a test, the values for a similar soil type can be used (see Table 2 for typical values).

Parameters, C and p , are influenced by grain compressibility. In addition, the state of packing affects the value of C as shown on Figure 7. These relationships can be used in the absence of material specific test data. For granular soils with low to medium compressibility $p \approx 0.9$ and $p \approx 0.65$ for highly compressible soils.

Parameter R_f can be approximated by $R_f \approx 1 - 0.003 \times D_R$, where D_R is in percent. Examination of laboratory behavior of sands also indicate that irrespective of the soil type and state of packing $n_p \approx -0.5$ and $m_A \approx 2$ for undisturbed fluvially deposited sand.

INVERSE MODELING OF SBPMT

To keep the inverse problem simple, the estimates of model parameters (other than K_{SP}) obtained from the guidelines of the preceding sections are not refined further while fitting the stress-strain model to the SBPMT measurements. Thus the problem of

inverse modeling essentially involves iteration over K_{SP} and σ_h' to fit the model response to cavity expansion data. The initial estimate of σ_h' is obtained from lift-off pressure (i.e., the cavity pressure at which the cavity starts to deform) and other information including soil unit weight, depth of ground water table, stress history, and geologic knowledge. Schematic details of the calibration procedure is presented in Figure 8.

ESTIMATION OF TRIAXIAL BEHAVIOR

The stiffest and softest SBPMT cavity expansion data at J-Pit (a deposit of spigotted Syncrude Sand near Fort McMurray, Alberta) and KIDD # 2 (a natural channel deposit of Fraser River Sand near Vancouver, BC) were analyzed as plane strain problems using an explicit finite difference computer program (Cundall, 1992). The results of back-analysis are shown in Figure 9 and the initial and boundary conditions and inferred model parameters are listed in Table 3.

Undisturbed samples were extracted by ground freezing from J-Pit and KIDD # 2 and triaxial tests were conducted on these samples. Hofmann and Seg0 (1995, 1994) give the details of the ground freezing activities at J-Pit and KIDD # 2. Details on laboratory tests can be found in Vaid et al. (1996).

The computed stress-strain response of a single axisymmetric element set to deform as in an undrained triaxial test using the model parameters of Table 3 are presented in Figure 10 along with the laboratory data. Table 4 lists the initial conditions of

actual and simulated triaxial tests. The computed and measured stress-paths are shown in Figure 11. These results indicate an approximate agreement between the laboratory measurements and the triaxial response inferred from in-situ tests.

Similar estimates of laboratory triaxial response were obtained from SBPMT measurements from LL Dam. However, unlike J-Pit and KIDD # 2, for LL Dam, the laboratory tests were carried out after the results from SBPMT data analysis were on the official record. For details on site investigation at LL Dam and laboratory testing see Bigger and Robertson (1996) and Fear and Robertson (1997).

A-priori information available for making the predictions at LL Dam was limited to SBPMT and SCPTU measurements. No additional material specific information was available for back-analysis of SBPMT. Therefore, the available values of λ and μ for Hilton Mines tailings from Table 2 were used. Since mine tailings are often comprised of angular grains, C and p for highly compressible materials were used.

Figure 12 presents the LL Dam SBPMT data and the model response in cylindrical cavity expansion for the optimized parameter sets. The predicted triaxial response for the parameter sets inferred from SBPMT are also presented in Figure 12 together with the laboratory measurements on undisturbed (frozen) samples. As earlier, the agreement between the actual triaxial response and that inferred from SBPMT is reasonable.

A CASE HISTORY

Possible use of the stress-strain curves derived from in-situ tests is illustrated using a recent case history. At J-Pit, an 8 m high earth embankment was constructed upon a 10 m thick foundation of loose Syncrude Sand (Figure 13). The foundation was prepared in the loosest possible state by underwater deposition of sand tailings so as to make an attempt to trigger static liquefaction within the foundation by quick dumping of tailings behind the embankment. More details on the field test, which failed to induce any appreciable movement, can be found in Byrne et al. (1995).

The foundation at J-Pit was characterized by an average $(N_1)_{60}$ of 3 except for a 2 to 4 m thick layer near the top, where the average $(N_1)_{60}$ was 7. Correlations of Figure 1 would indicate a negligible undrained strength for such low values of SPT blow count. Using $s_u=1$ kPa for the foundation and idealizing the tailings dumped behind the embankment as a material without any shear strength, one gets a limit equilibrium (Bishop, 1955) factor of safety of 0.04: a value that would suggest static liquefaction.

The procedure described in this paper, on the other hand, indicates that the lower bound strength of the surficial layer is approximated by $s_u \approx 0.25 \times \sigma_{vo}'$ in plane strain extension and $0.58 \times \sigma_{vo}'$ in plane strain compression. The corresponding values for the deeper layers of loose sand are $0.04 \times \sigma_{vo}'$ and $0.58 \times \sigma_{vo}'$, respectively. The undrained strength was assumed to be equal to one half of the deviator stress at the Steady State for strain softening materials, and that at Quasi Steady State for partially strain softening

material response. Undrained shear strength at Phase Transformation was used for strain hardening materials. Using these estimates of shear strength, a static Bishop factor of safety of 1.7 was obtained: a value that is in qualitative agreement with the observed lack of movement during the field experiment.

IMPLICATIONS

The problem with the use of $(N_1)_{60}$ as an index of undrained strength of sand was recognized by Castro (1995). Castro suggests that the lower bound correlation between $(N_1)_{60}$ and s_u should only be relied upon to identify deposits that are potentially prone to static liquefaction and recommends a detailed laboratory investigation once potentially liquefiable deposits have been identified to verify the SPT based inference. The illustrative example of the preceding section indeed indicates that use of Seed's lower-bound relationship for estimating the undrained strength may be over-conservative. However, extraction of undisturbed samples from sand deposits and laboratory testing can be very expensive. From the results presented above it appears that back-analysis of SBPMT can provide an economic alternative.

CONCLUSIONS

A procedure is developed for approximate calibration of a stress-strain model for granular deposits from in-situ test data. The computed undrained triaxial response using the optimized set of model parameters obtained from the calibration process was found to

compare reasonably with the observed laboratory behavior of undisturbed samples. These results indicate that the proposed method can be useful in assessing the static liquefaction potential; a problem in which the commonly used empirical procedures based on in-situ index tests such as SPT and CPTU tend to be over-conservative.

ACKNOWLEDGEMENTS

This study was partly funded by the Canadian Liquefaction Experiment (CANLEX), a research undertaking of several educational institutions, industrial participants, and Natural Sciences and Engineering Research Council of Canada (NSERC). The first author also would like to thank UBC for financial support through University Graduate Fellowship.

APPENDIX. REFERENCES

- Arthur, J.R.F., and Menezies, B.K. 1972. Inherent anisotropy in a sand. *Géotechnique*, 22, 115-128.
- Basudhar, P.K. and Kumar, D. 1995. Performance studies of cavity expansometer: a monocell pressuremeter. *The Pressuremeter and its New Avenues*. Ballivy, G., Ed., Balkema, Rotterdam, the Netherlands, 73-30.
- Bigger, K.W., and Robertson, P.K. 1996. Phase IV detailed site characterization. *CANLEX Rep.* Dept. of Civil Engrg., Univ. of Alberta.

- Bishop, A.W. 1955. The use of the slip circle in the stability analysis of slopes. *Géotechnique*, 5, 7-17.
- Bishop, A.W. 1952. Shear characteristics of a saturated silt, measured in triaxial compression: correspondence. *Géotechnique*, 2, 43-45.
- Bolton, M.D. 1986. The strength and dilatancy of sands. *Géotechnique*, 36, 65-78.
- Bruzzi, D., Ghionna, V., Jamiolkowski, M., Lancellotta, R., and Manfredini, G. 1986. Self-boring pressuremeter in Po river sand. *Proc., Pressuremeter and its Marine Application, STP 950, ASTM*, 283-302.
- Byrne, P.M., Robertson, P.K., Plewes, H.D., List, B., and Tan, S. 1995. Liquefaction event planning. *Proc., 48th Canadian Geotech. Conf., Vancouver*, 1, 341-352.
- Cunning, J.C., Robertson, P.K. and Segoo, D.C. 1995. Shear wave velocity to evaluate in-situ state of cohesionless soils. *Canadian Geotech. J.* 32, 848-858.
- Castro, G. 1995. Empirical methods in liquefaction evaluation. *Primer Ciclo de Conferencias Internacionales Leonardo Zeevaert. Mexico City.*
- Cundall, P.A. 1992. *FLAC ver. 3.0: user's manual.* Itasca Consulting Group, Minneapolis, Minnesota.
- da Cunha, R.P. 1994. Interpretation of selfboring pressuremeter tests in sand. *Ph.D. Dissertation, Univ. of BC.*

- Fahey, M., and Carter, J.P. 1993. a finite element study of the pressuremeter test in sand using non linear elastic plastic model. *Canadian Geotech. J.*, 30, 348-362.
- Fear, C.E., and Robertson, P.K. 1995. Phase IV Data Review Report. *CANLEX Rep.* Dept. of Civil Engrg., Univ. of Alberta.
- Fear, C.E., and Robertson, P.K. 1995. Estimating the undrained strength of sand: a theoretical framework. *Canadian Geotech. J.*, 32, 859-870.
- Fioravante, V., Jamiolkowski, M., and Lo Presti, D.C.F. 1994. Stiffness of Carbonic Quiou Sand. *Proc.*, XIII Int. Conf. on Soil Mechanics and Foundation Engrg., 1, 163-167.
- Hardin, B.O. 1978. Stress-strain behavior. *Proc.*, Earthquake Engrg. and Soil Dynamics, ASCE, 1, 3-90.
- Hofmann, B.A., and Seg0, D.C. 1994. Phase II - Activity 4B: In-situ ground freezing and sampling at the Phase II test site. *CANLEX Rep.* Dept. of Civil Engrg., Univ. of Alberta.
- Hofmann, B.A., and Seg0, D.C. 1995. Phase III - Activity 4B: In-situ ground freezing and sampling at the Phase III event site. *CANLEX Rep.* Dept. of Civil Engrg., Univ. of Alberta.
- Hughes, J.M.O., Wroth, C.P., and Windle, D. 1977. Pressuremeter tests in sands. *Géotechnique*, 27, 455-477.
- Lade, P.V. 1977. Elasto-plastic stress-strain theory for cohesionless soil with curved yield surfaces. *Int. J. of Solids and Structures*, 13, 1019-1035.

- Lade, P.V., and Nelson, R.B. 1987. Modelling the elastic behaviour of granular materials. *Int. J. for Numerical and Analytical Methods in Geomechanics*, 11, 521-542.
- Nakai, T., and Matsuoka, H. 1983. Shear behaviors of sand and clay under three-dimensional stress condition. *Soils and Foundations*, 23(2), 26-42.
- Oda, M. 1972. Initial fabrics and their relations to mechanical properties of granular material. *Soils and Foundations*, 12(1), 17-37.
- Pass, D.G. 1994. Soil characterization of the deep accelerometer site at Treasure Island, San Francisco, California. *MS Thesis*, Univ. of NH.
- Poorooshasb, H.B., and Roscoe, K.H. 1961. The correlation of the results of shear test with varying degree of dilation. *Proc.*, V Int. Conf. on Soil Mechanics and Foundation Engrg., 1, 297-304.
- Robertson, P.K., and Campanella, R.G. 1986. Guidelines for use, interpretation and application of the CPT and CPTU. *Soil Mechanics Series No. 105*. Dept. Of Civil Engrg. Univ. Of BC.
- Roy, D., Campanella, R.G., Byrne, P.M., and Hughes, J. 1996. Strain level and uncertainty of liquefaction related index tests. *Uncertainty in the Geologic Environment: from Theory to Practice*, Shackelford, C.D., Nelson, P.P., and Roth, M.J.S., eds., Special Technical Publication No. 58, ASCE, 2, 1149-1162.
- Roy, D. 1997. Deformation behavior of granular deposits from self-boring pressuremeter, *Ph.D. Dissertation*, Univ. of BC.

- Seed, H.B., Seed, R.B., Harder, L.F., and Jong, H.-L. 1988. Reevaluation of the slide in the Lower Sand Fernando Dam in the earthquake of February 9, 1971. Rep. No. UCB/EERC-88/04, Univ. of California, Berkeley.
- Tatsuoka, F., and Kohata, Y. 1995. Stiffness of hard soils and soft rocks in engineering applications. Rep., Institute of Industrial Science, Univ. of Tokyo.
- Tatsuoka, F., Sakamoto, M., Kawamura, T., and Fukushima, S. 1986. Strength and deformation characteristics of sand in plane strain compression at extremely low pressures. *Soils and Foundations*, 26(1), 65-84.
- Vaid, Y.P., Sivathayalan, S., Eliadorani, A., and Uthayakumar, M. 1996. Laboratory testing at U.B.C. and Addendum to Appendix 6. *CANLEX Rep.* Dept. of Civil Engrg., Univ. of Alberta.
- Verdugo, R.L. 1992. Characterization of sandy soil behavior under large deformation. *Ph.D. Dissertation*, Univ. of Tokyo.
- Yoshimine, M. 1996. Undrained flow deformation of saturated sand under monotonic loading conditions. *Ph.D. Dissertation*, Univ. of Tokyo.
- Yu, H.S. 1994. State parameter from self-boring pressuremeter tests in sand. *J. Geotech. Engrg.*, ASCE, 120, 2118-2135.

TABLE 1.- Elastic Model Parameters

Sand type (1)	D_{Rf} % (2)	K_{GE} (3)	n_E (4)	Location (5)	Reference (6)
Ottawa C109	70	1260	0.5		Cunning et al. (1995)
	50	1080	0.5		Ditto
	30	910	0.5		Ditto
Quiou (carbonate) Sand	59	995	0.7		Fioravante et al. (1994)
	53	845	0.7		Ditto
Fraser River Sand	38	750	0.5	Massey	This study
	50	950	0.5	KIDD # 2	Ditto
Syncrude Sand	65	550	0.5	Cell 24	Ditto
	30	450	0.5	J-Pit	Ditto

TABLE 2.— Model Parameters Associated with Plastic Flow

Soil Type (1)	λ (2)	μ (3)
Erksak Sand	0.83	0.30
Fraser River Sand	0.77	0.39
Hilton Mines Tailings	0.80	0.40
Ottawa C109	0.85	0.26
Syncrude Sand	0.85	0.29
Ticino Sand	0.87	0.33
Toyoura Sand	0.90	0.27

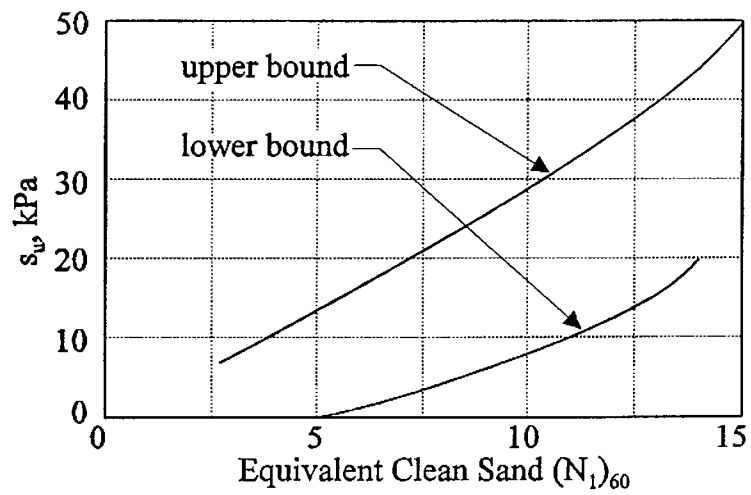
TABLE 3.- Model Parameters from SBPMT

Site	Depth	D_{R1}	σ_{vo}'	K_0	K_{GE}	η_{F1}	$\Delta\eta$	K_{SP}	R_F
(1)	(2)	(3)	(4)	(5)	(6)	(7)	(8)	(9)	(10)
J-Pit	4.53	~30	44	0.5	400	0.52	0.01	175	0.98
	5.18	~60	54	0.5	500	0.62	0.06	1000	0.87
KIDD # 2	14.37	~30	137	0.5	750	0.71	0.06	240	0.98
	16.38	~65	155	0.7	1100	0.79	0.10	1000	0.82

TABLE 4.— Particulars of Triaxial Tests

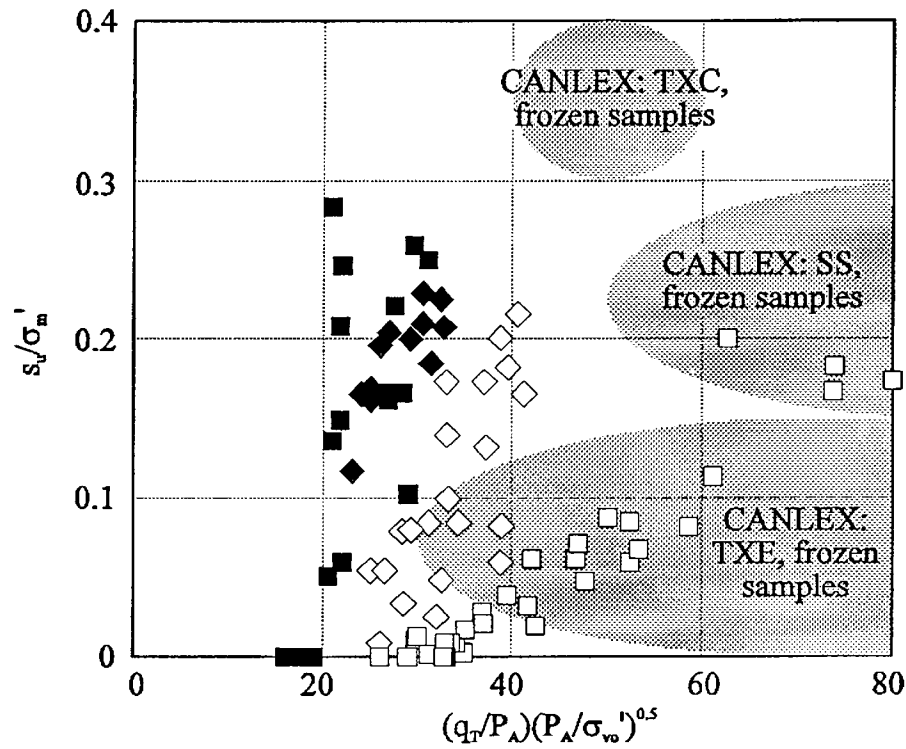
Site	Test No.	D_R , %	σ'_{VCONS} kPa	Type
(1)	(2)	(3)	(4)	(5)
J-Pit	FS5C1B31	31	44	TXE
	FS5C1B33	31	204	TXC
	FS26C211	58	40	TXE
	FS6C2B24	66	48	TXC
KIDD # 2	K94F1C70	67	150	TXE
	K94F1C23	53	120	TXC
	K94F3C4B2	36	156	TXE
	K94F2C2A	40	145	TXC

Notes: 1. σ'_{VCONS} = effective vertical stress at the beginning of test
2. σ'_{HCONS} = effective vertical stress at the beginning of test = $0.5 \sigma'_{VCONS}$



Note: the undrained strengths in this figure are back calculated values from post-failure geometry

FIG. 1.— Relationship Between s_u and $(N_1)_{60}$ Proposed by Seed et al. (1988)



- Moist Tamped Toyoura Sand in Triaxial Compression (Verdugo, 1992)
- ◆ Air Pluviated Toyoura Sand in Triaxial Compression (Yoshimine, 1992)
- ◇ Air Pluviated Toyoura Sand in Simple Shear (Yoshimine, 1992)
- Air Pluviated Toyoura Sand in Triaxial Extension (Yoshimine, 1992)

Note: The undrained strengths in this figure are at steady state or at phase transformation

FIG. 2.— Effect of Stress Path and Inherent Anisotropy on the s_u - q_T Relationship

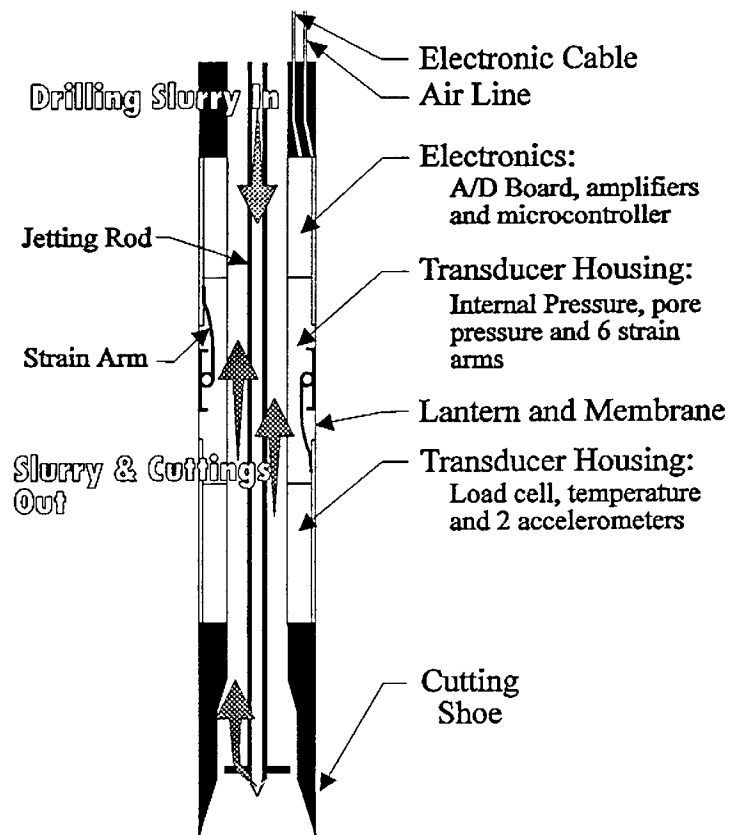


FIG. 3.— Schematic Details of the Self-boring Pressuremeter Probe

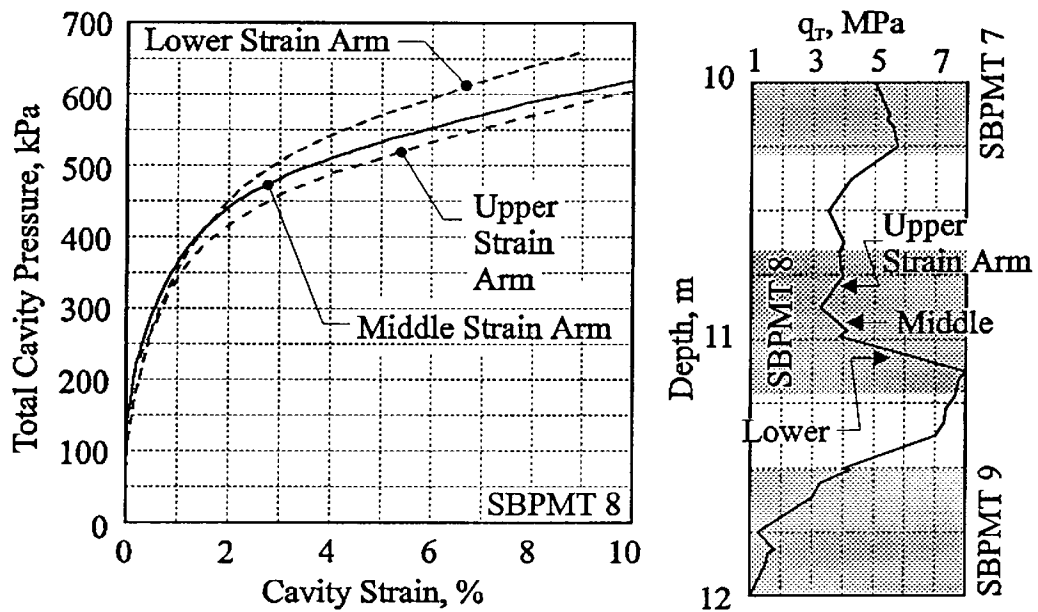


FIG. 4.— End Effects

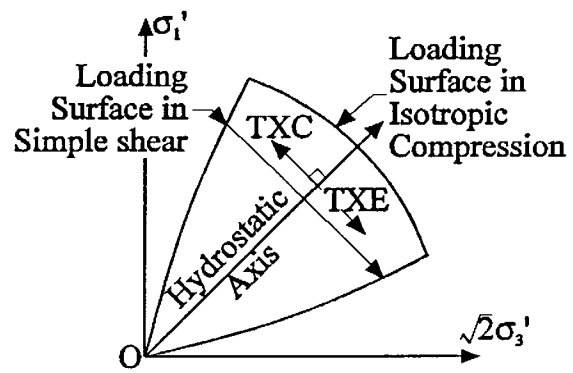
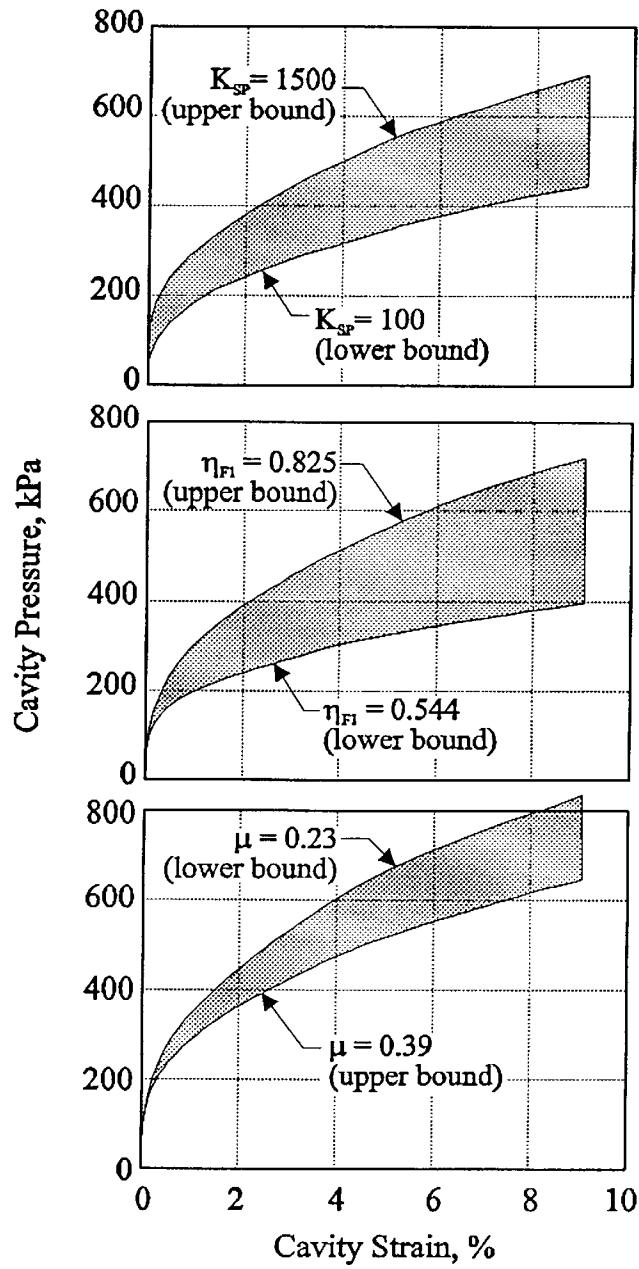


FIG. 5.— Loading Surfaces



Baseline: $K_{GE}=500$, $n_E=0.5$, $\nu=0.2$, $K_{SP}=500$, $n_P=-0.5$, $\eta_{FI}=0.75$, $\Delta\eta=0.08$, $\lambda=0.77$, $\mu=0.39$, $R_F=0.85$, $C=0.0004$, $p=0.9$, $m_A=2$

FIG. 6.— Sensitivity of Cylindrical Cavity Expansion to the Choice of K_{SP} , η_{FI} and μ

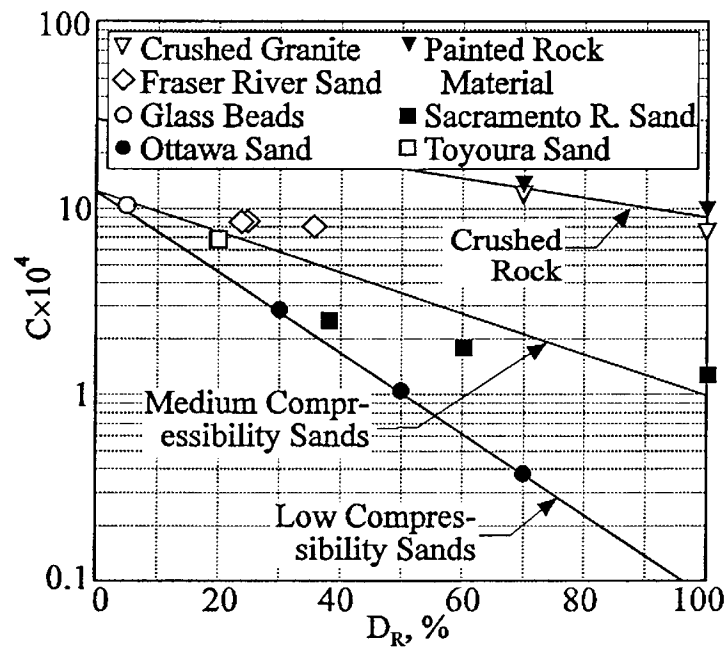


FIG. 7.— Parameter "C" as a Function of Relative Density and Grain Compressibility

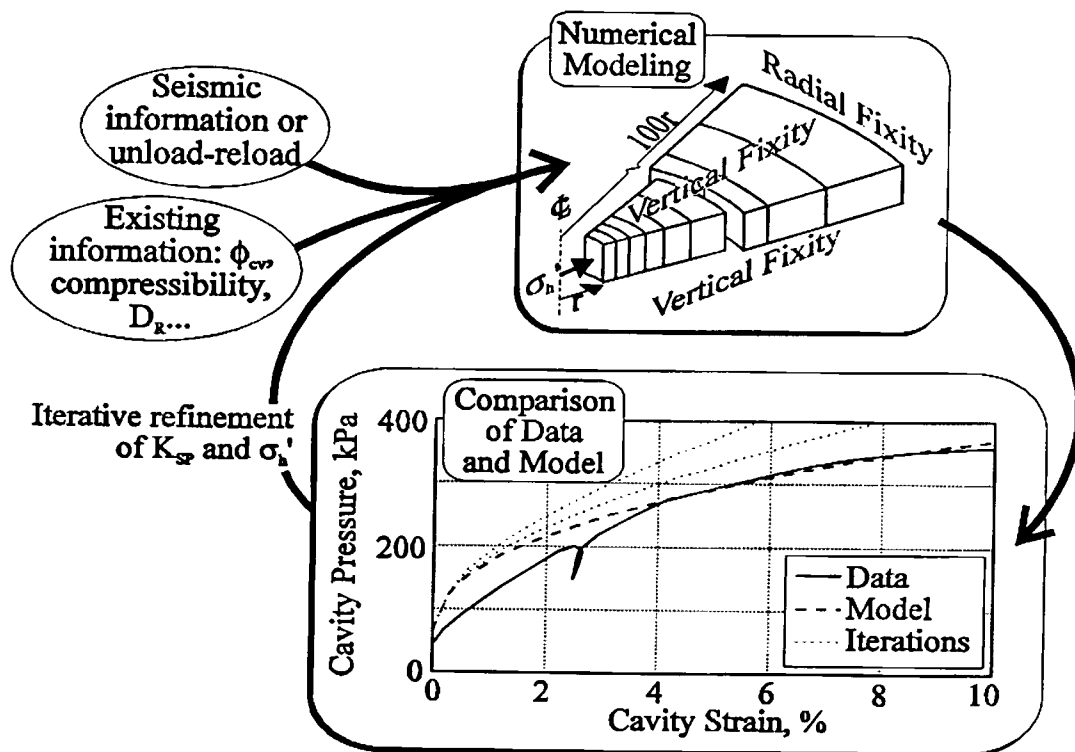


FIG. 8.- Procedure for Back-analysis of SBPMT

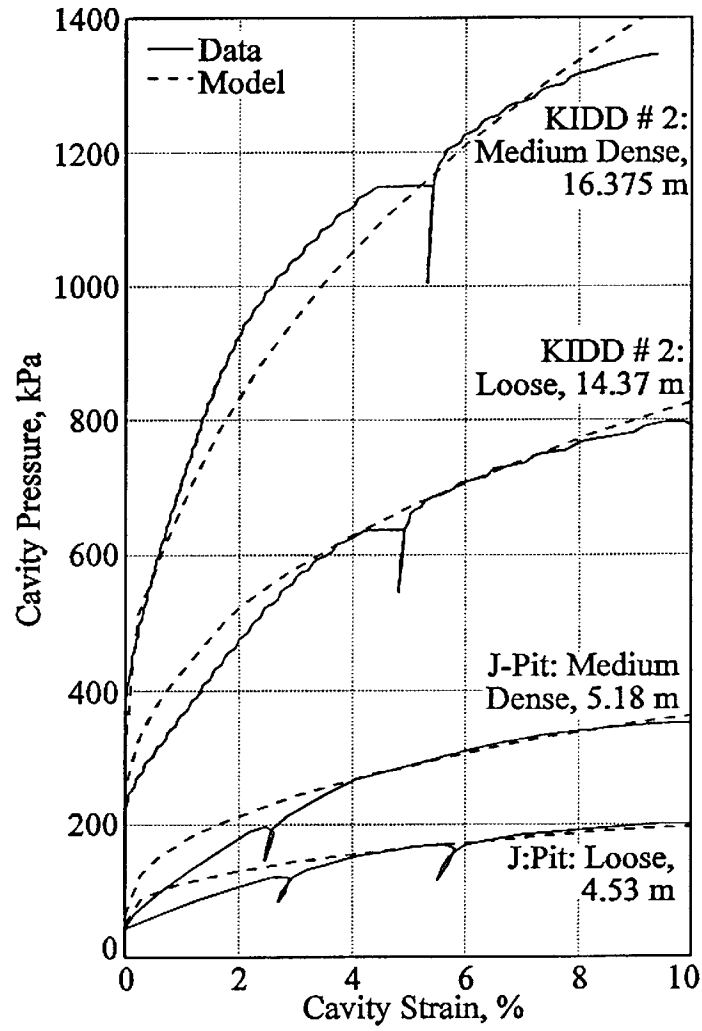


FIG. 9.— Results of Back-analysis of SBPMT Data

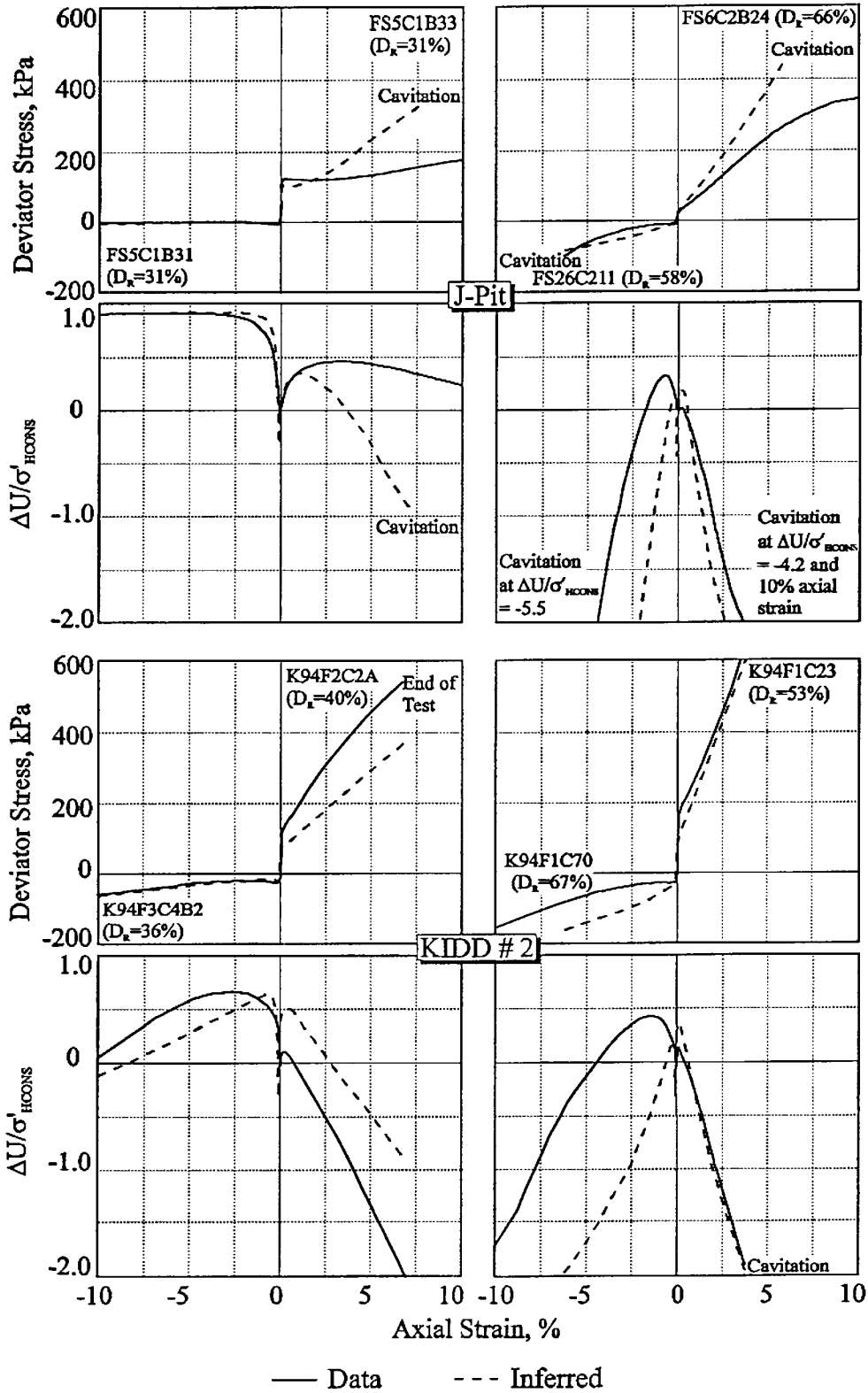
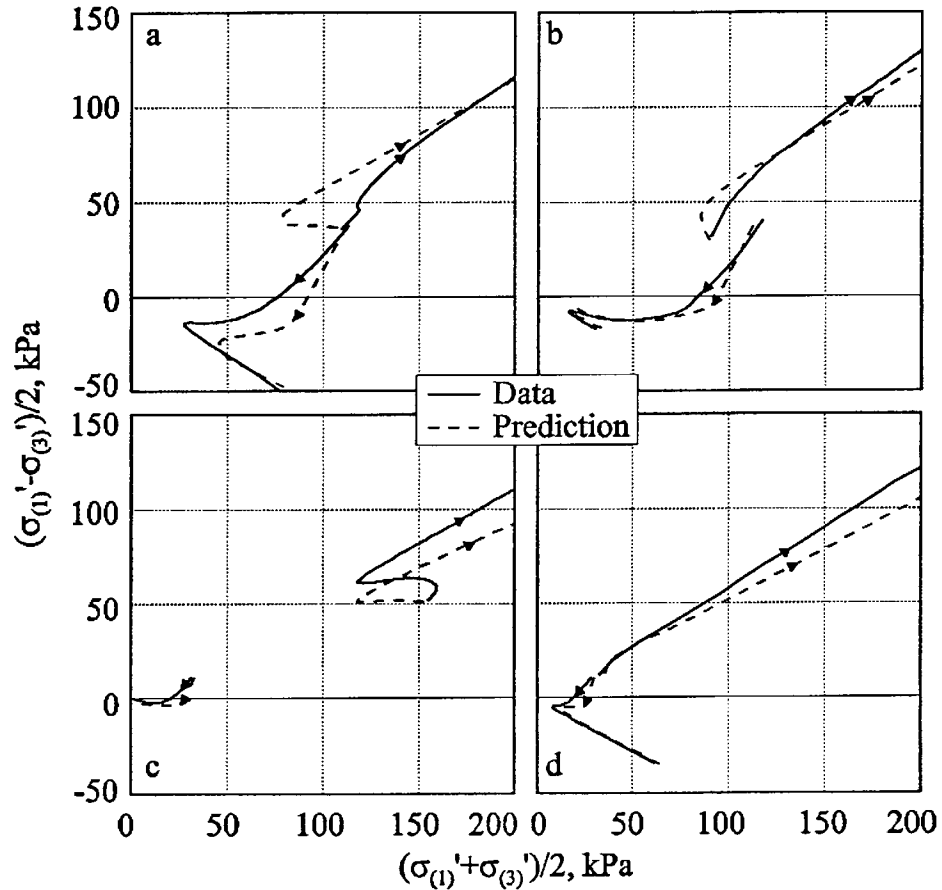


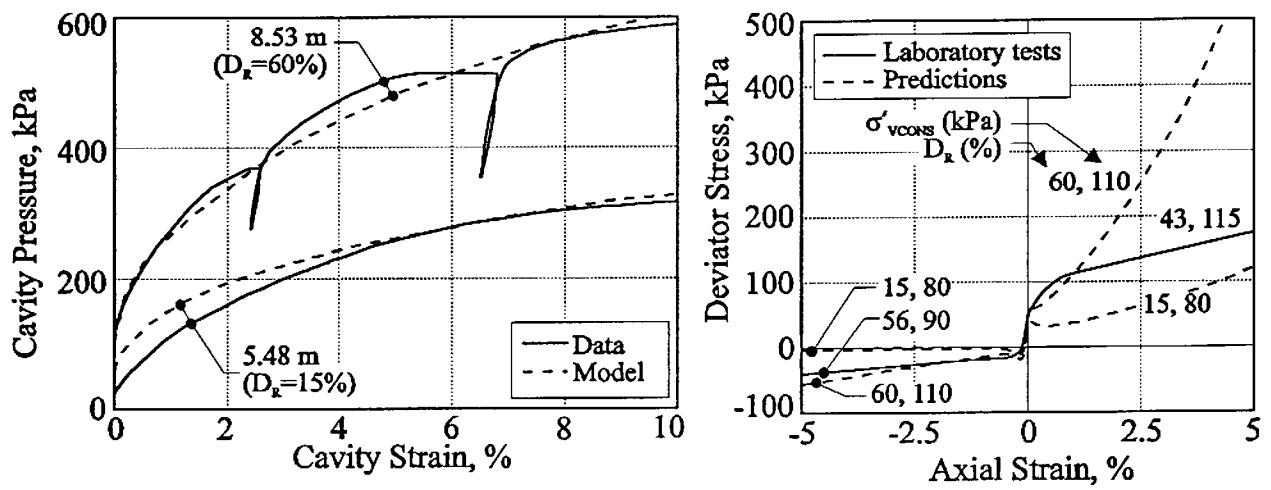
FIG. 10.— Measured and Inferred Triaxial Stress-strain Behavior



- a. KIDD # 2: K94F3C4B2 ($D_R=36\%$) and K94F2C2A ($D_R=40\%$)
- b. KIDD # 2: K94F1C70 ($D_R=67\%$) and K94F1C23 ($D_R=53\%$)
- c. J-Pit: FS5C1B31 ($D_R=31\%$) and FS5C1B33 ($D_R=31\%$)
- d. J-Pit: FS26C211 ($D_R=58\%$) and FS6C2B24 ($D_R=58\%$)

Note: $\sigma_{(1)}$ ' and $\sigma_{(3)}$ ' are the major and minor effective principal stresses

FIG. 11.— Measured and Inferred Triaxial Stress-paths



Note: $\sigma'_{HCONS} = 0.5 \times \sigma'_{VCONS}$

FIG. 12.— Class "A" Prediction of LL Dam Triaxial Response

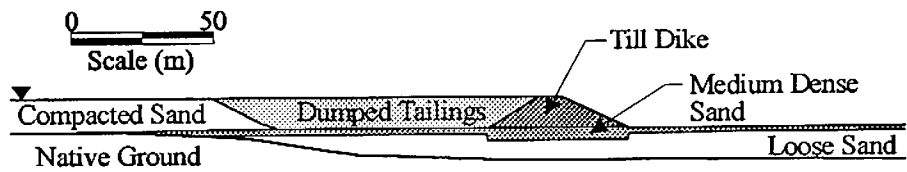


FIG. 13.- CANLEX Static Liquefaction Experiment